5-1-2011

Interpretation of Rayleigh-Wave Ellipticity Observed with Multicomponent Passive Seismic Interferometry at Hekla Volcano, Iceland

Matthew M. Haney
Boise State University

Andrew Nies
Boise State University

Tim Masterlark
University Of Alabama

Sarah Needy
University Of Alabama

Rikke Pedersen
University of Iceland

Interpretation of Rayleigh-wave ellipticity observed with multicomponent passive seismic interferometry at Hekla Volcano, Iceland

Matthew M. Haney and Andrew Nies, Boise State University
Tim Masterlark and Sarah Needy, University of Alabama
Rikke Pedersen, University of Iceland

The 2010 eruption of Eyjafjallajökull has drawn increased attention to Iceland's Eastern Volcanic Zone (EVZ) due to the threat it poses to the heavily used air-traffic corridors of the northern Atlantic Ocean. Within the EVZ, Hekla is historically one of the most active volcanoes and has exhibited a decadal eruption pattern for the past 40 years. Hekla most recently erupted in 2000 and is thus ripe for another decadal eruption. Because Hekla is generally aseismic, except for a brief time period (hours) leading up to an eruption, monitoring has previously depended on precursory deformation signals (Linde et al., 1993). As a result, seismic tomography of the internal structure of the volcano using phase arrivals of local earthquakes is not possible. Motivated by Hekla's practically aseismic behavior in inter-eruptive periods, we installed a temporary network of four broadband seismometers around the volcanic edifice in late August 2010 with the intention of investigating the applicability of passive seismic interferometry (PSI) for imaging and monitoring the volcano.

In frequency bands below 1 Hz, PSI benefits greatly from the pervasive and continuous noise sources arising from the coupling of the oceans to the solid Earth (Lin et al., 2008; Masterlark et al., 2010). These noise sources are referred to as the oceanic microseism, a term not to be confused with microseismicity or small earthquakes. PSI is best known as a part of the technique called ambient noise tomography (ANT). Ambient noise tomography encompasses three separate steps: PSI, surface-wave tomography, and depth imaging. PSI pertains to the cross-correlation process between pairs of receivers. Applying the multiple filter technique (Lin et al., 2008) to these cross-correlations yields a set of path-averaged dispersion curves between each receiver pair within a network. These path-averaged dispersion curves can alternatively be viewed as a set of group traveltime tables for each frequency. The second step, surface-wave tomography, takes the traveltime tables for each frequency and returns lateral maps of group velocity at each frequency. Finally, the depth-imaging step inverts local dispersion curves at each lateral point for a local depth structure, resulting in a 3D image of shear-wave velocity.

The earliest implementations of ANT used cross-correlations between only vertical components. Recently, Lin et al. discussed how to extend the cross-correlations to three-component seismometers for the purpose of obtaining Rayleigh- and Love-wave dispersion. Here, we implement this technique of multicomponent PSI on a network of four broadband seismometers at Hekla Volcano in Iceland. We demonstrate the ability of multicomponent PSI for obtaining both vertical and radial Rayleigh-wave seismograms between stations. Because relative amplitudes on a three-component seismometer are preserved in multicomponent PSI, we are able to quantitatively analyze the ellipticity of the Rayleigh-wave particle-motion, also called the HZ ratio. The HZ ratio is known to possess information on shallow shear-wave velocity structure beneath a receiver (Tanimoto and Tsuboi, 2009) that is independent from information derived from group velocity dispersion. The HZ ratio can be theoretically shown to be a pure site effect, meaning that it does not vary within common receiver gathers. We find that this property of the HZ ratio holds only

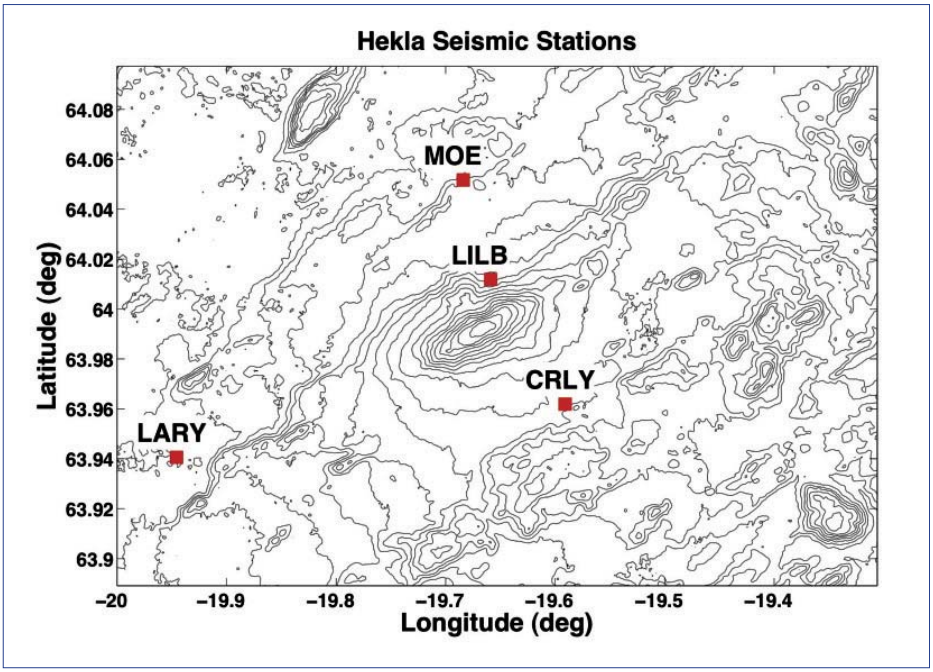

Figure 1. *A topographic map centered on Hekla Volcano, Iceland, showing the locations of the temporary seismometers. The summit of the volcano lies just south of station LILB.*

Figure 2. *Hekla Volcano viewed from the southeast, near the site CRLY. The vantage point is normal to the main fissure of the volcano. The lava flow in the foreground is from the 1991 eruption.*

within a narrow frequency band at Hekla. However, the additional information provided by the HZ ratio in this narrow band further constrains the shallow shear velocity structure at Hekla. These results show that HZ ratio, in addition to velocity dispersion, can become a primary observable for imaging and monitoring the subsurface in future applications of PSI.

Field deployment

The temporary network at Hekla consists of two Guralp 3-ESPDs (stations LARY and MOE) and two Guralp 40-Ts (stations CRLY and LILB). The station locations are shown in Figure 1. Stations MOE, LILB, and CRLY are powered to acquire data from August 2010 until July 2011 and each sits on a small, level pad of concrete that is coupled to the bedrock. Power is provided by two strings of five air-cell type batteries connected in parallel and stored on site in a 48-gallon plastic container. Station LARY is in a small shed with access to electricity and therefore does not use battery power. Within the network, station LILB lies less than 3 km from the main eruptive fissure on the northeastern slope of the volcano. The three other instruments are 5–15 km from the summit of Hekla to provide good azimuthal coverage. The photograph in Figure 2 shows the view of Hekla from station CRLY, where the volcanic edifice appears as a broad shield. Hekla is elongated along a SW-NE trending fissure and the volcano looks more like a stratovolcano when viewed from the southwest. Also shown in Figure 2 is the toe of the lava flow emplaced during the 1991 eruption, at a distance of approximately 5 km from the eruptive fissure.

Data processing

A typical amplitude spectrum of ambient seismic noise recorded at station LARY is given in Figure 3. The oceanic microseism dominates the signal between 0.15 and 0.5 Hz.

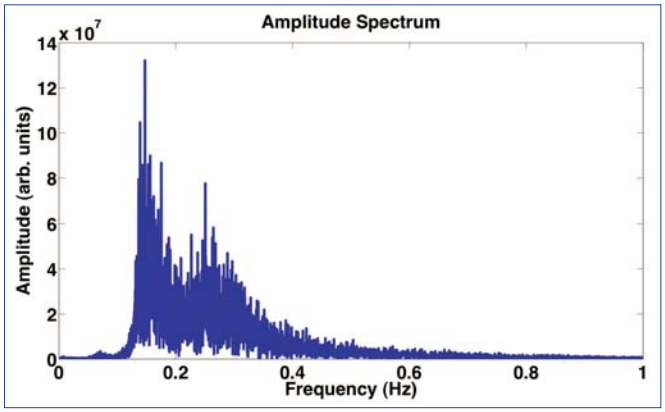

Figure 3. *Amplitude spectrum at station LARY for typical noise during an hour without earthquakes or other large signals. The ocean noise registers between frequencies of approximately 0.15–0.5 Hz, with peaks at 0.15 Hz and 0.3 Hz. Notice also the small peak at a frequency below 0.1 Hz.*

Thus, we can expect PSI to work well within this frequency band. We apply PSI to the first 52 days of continuous recordings, which began on 28 August 2010, from the local network of four three-component seismometers. The fact that the seismometers are all three-component instruments means a multicomponent version of PSI can be implemented. Lin et al. recently discussed the details of multicomponent PSI. The main difference with conventional single-component PSI is that the temporal-normalization and spectral-whitening filters must be applied identically across all three components (NS, EW, and UD) in order to preserve the relative amplitudes. This means that the popular sign-bit type of temporal normalization must be avoided and instead replaced by a type of multichannel automatic gain control (Masterlark et al., 2010). By applying multicomponent PSI to the Hekla seismic data, we are able to analyze cross-correlations between pairs of vertical components (ZZ), radial components

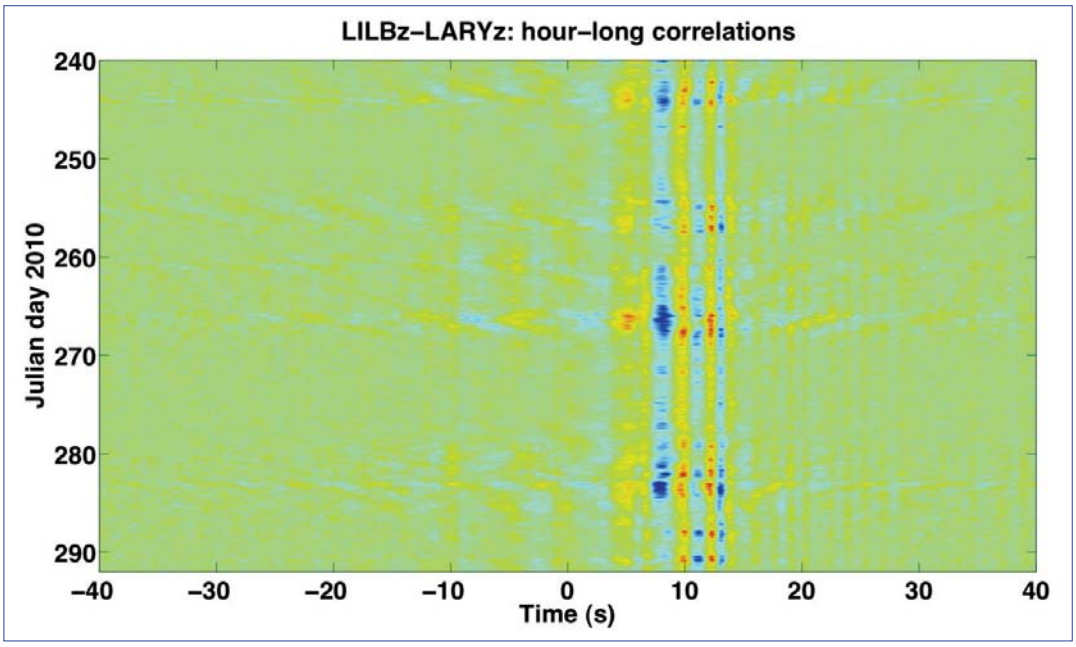

Figure 4. *Continuous, hour-long correlations between vertical components for stations LILB and LARY over 52 days. The waveform at positive time lags is observed to have variable amplitude over the 52 days but a more or less stable arrival time.*

(RR), transverse components (TT), and mixtures of vertical and radial components (ZR). Rayleigh waves propagating between stations are captured on the ZZ, RR, and ZR correlations; Love waves appear on the TT correlations. Therefore, with multicomponent PSI, one can analyze two independent modes of wave propagation, as has been shown by Lin et al. Masterlark et al. previously used multicomponent PSI at Okmok Volcano to image the subsurface magma chamber with Rayleigh waves using ZZ, ZR, and RR correlations.

With four stations deployed at Hekla, there are four transverse and eight vertical/radial channels possible. This yields 6 (= 4 × 3/2) and 24 (= 8 × 7/2 – 4) different cross-correlations for Love and Rayleigh waves, respectively. Note that the four cross-correlations between the vertical and radial component from the same seismometer are not used to analyze Rayleigh waves. In principle, the group traveltimes of Rayleigh waves picked from ZZ, RR, and ZR correlations between a station pair should be the same. This is because the group traveltime concerns the envelope of the wave train, which is insensitive to any 90° phase shifts between the Z and R components. With noisy data, the ZZ, RR, and ZR correlations provide independent estimates of the group traveltime.

Hour-long cross-correlations for the channel pair LILBz and LARYz over the first 52 days of the deployment are plotted in Figure 4. The cross-correlation is asymmetric and contains a Rayleigh wave at positive time lags, indicating the direction to the ocean noise source. Although the amplitude of the waveform varies, its arrival time is generally repeatable over the 52 days. A robust estimate of the cross-correlation for LILBz–LARYz can be obtained by averaging the hour-long cross-correlations over the entire 52 days.

HZ ratio

We focus our analysis on the following six cross-correlations: MOEz–LARYz, MOEz–LARYr, LILBz–LARYz, LILBz–LARYr, and CRLYz–LARYz, CRLYz–LARYr. These pairs include all possible combinations of vertical components in the network with the vertical and radial components from station LARY. We estimate the HZ ratio at LARY by comparing the amplitudes of cross-correlations that share a vertical component in the network and include both LARYz and LARYr. For instance, LILBz–LARYz and LILBz–LARYr together give one estimate of the HZ ratio. In addition, we can obtain two more estimates of the HZ ratio at LARY from the other cross-correlations. These three independent estimates of HZ ratio motivate a test to see if this quantity is truly a site effect, with negligible variability within the common receiver gather.

In Figure 5, we overlay the cross-correlations for LILBz–LARYz and LILBz–LARYr. The 90° phase shift between the two traces is clearly evident, guaranteeing that this is a Rayleigh-wave arrival. Also seen in Figure 5 is the presence of strong dispersion for the Rayleigh wave—the beginning of the wave train is dominated by low frequencies that merge into higher frequencies at the end. These two cross-correlations can be analyzed using the multiple-filter technique (Lin et al.) in order to study their group-velocity spectra. These spectra are depicted in Figure 6 together with the group velocity dispersion curve picked along the maximum of the spectrum. Note that the dispersion curves computed from the two spectra are within 2–3% of each other. Also notice that the LILBz–LARYz correlation is higher in amplitude than LILBz–LARYr correlation over the frequency band 0.15–0.5 Hz. This indicates that the HZ ratio is less than 1 at station LARY.

To measure the HZ ratio, we in essence sum along columns of both group velocity spectra in Figure 6 and take the ratio between LILBz–LARYr and LILBz–LARYz at each frequency. Because the vertical axis in the group velocity spectra is a distorted traveltime axis, the summation is actually

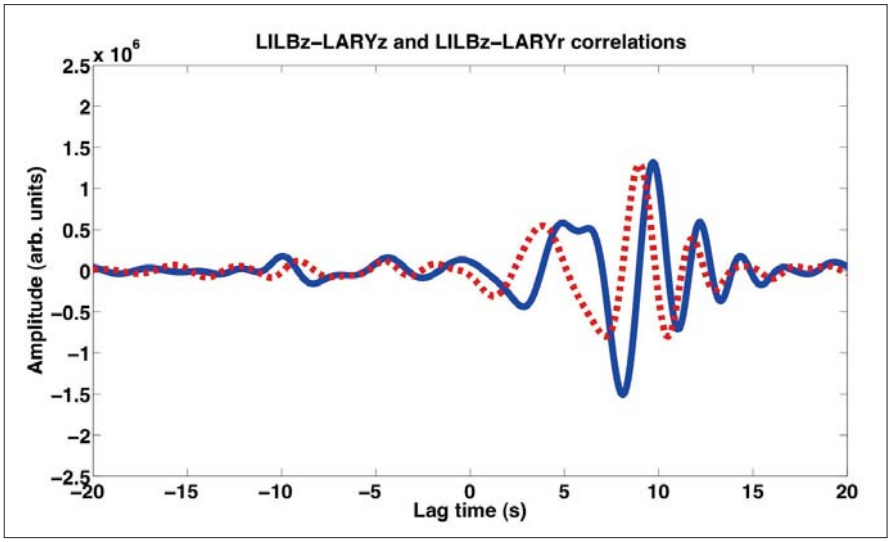

Figure 5. *Vertical (solid blue) and radial (dashed red) cross-correlation traces measured at LARY from the vertical component at LILB. The distinctive 90° phase shift characteristic of Rayleigh waves is evident, as well as significant velocity dispersion.*

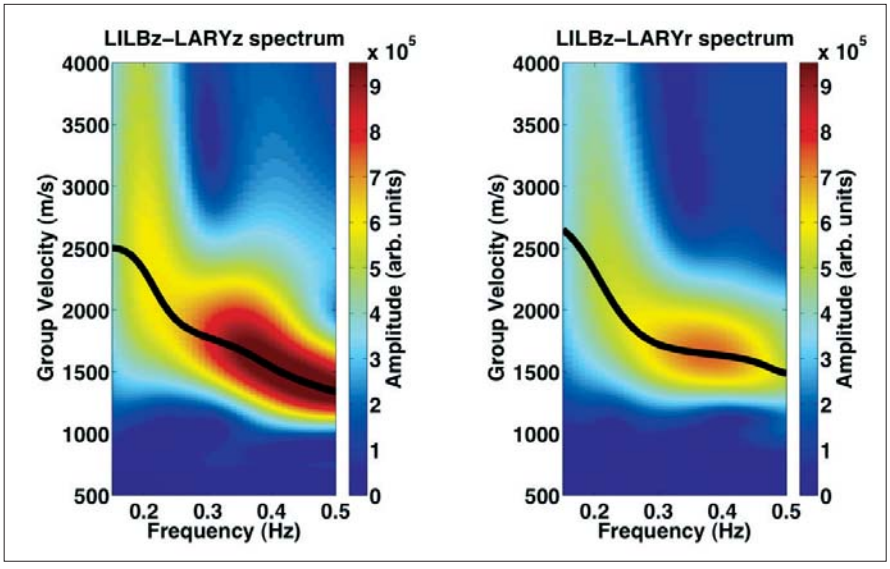

Figure 6. *Group velocity spectra for the pairs LILBz–LARYz and LILBz–LARYr. The peak of the spectra, the group velocity dispersion curve, is also plotted as a black line.*

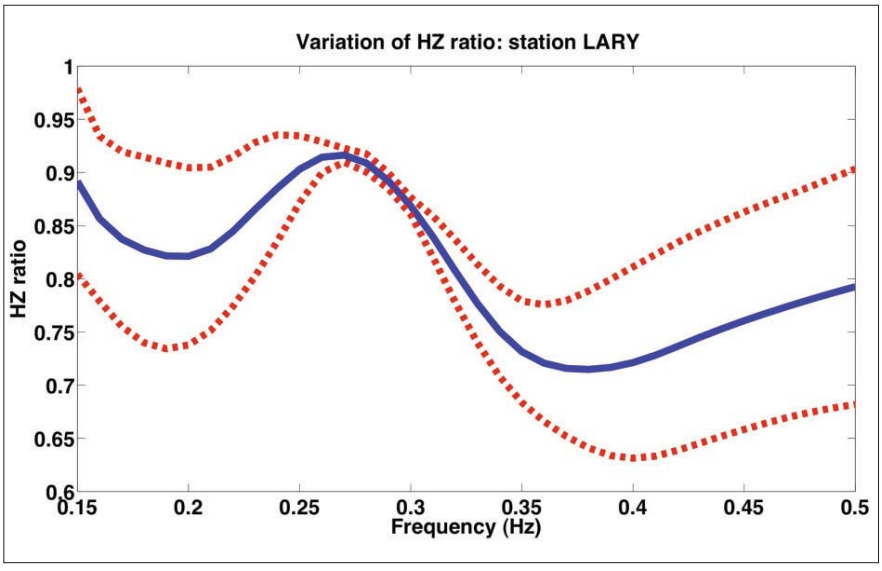

Figure 7. *The average HZ ratio (solid blue) at station LARY plotted along with error bars equal to 1 standard deviation (dashed red). The HZ ratio is seen to be highly consistent at LARY for the different station pairs at 0.28 Hz. Outside of the band 0.25–0.35 Hz, the HZ ratio varies significantly*

done in the traveltime domain with only minor differences. This technique is robust, provided that the summation includes only the direct wave propagating between the receivers. This assumption is satisfied within the band 0.15–0.5 Hz. After computing the HZ ratio at station LARY from the other two stations in the network, we obtain three independent estimates of the HZ ratio. From these independent estimates, we plot (Figure 7) their mean over the frequency band 0.15–0.5 Hz along with error bars of one standard deviation. It is evident from Figure 7 that the HZ ratio at LARY varies significantly between the three independent estimates except within a narrow band of frequencies from 0.25 to 0.35 Hz. This demonstrates that the HZ ratio is not necessarily a pure site effect, as predicted theoretically (Tanimoto and Tsuboi). We speculate that, for frequencies higher than 0.35 Hz, topographic and perhaps scattering effects distort the HZ ratio. Similarly, at frequencies below 0.25 Hz, the far-field assumption used to show that the HZ ratio is a pure site effect (Aki and Richards, 1980) may become less reliable. Therefore, the frequency band 0.25–0.35 Hz provides a narrow window over which reliable HZ ratio information can be obtained at Hekla.

Interpretation

With the estimated mean and standard deviations of the HZ ratio at LARY, we can find a shear-wave velocity model beneath LARY that explains the observations within the uncertainties of the measurements. Note that the ability to obtain multiple independent estimates of the HZ ratio at LARY allows the variability of the estimates to be captured within an inverse analysis. To do so requires that we set up an inversion for the HZ ratio of Rayleigh waves. HZ ratio inversion is not trivial and has been formulated only recently by Tanimoto and Tsuboi. It is similar in some ways to dispersion curve inversion; however, the HZ ratio is known to have an even shallower depth of sensitivity. For the frequency band 0.15–0.5 Hz, we find that there is acceptable resolution to depths of 3–4 km at Hekla. The inversion of HZ ratio, denoted R, is based on a perturbational theory (Tanimoto and Tsuboi) that relates perturbations in R to perturbations in a shear-wave velocity profile β through a sensitivity matrix $\boldsymbol{K}$:

$$\Delta R/R = \mathrm{K}\,\Delta\beta/\beta \qquad (1)$$

We perform this inversion using a simple damped least-squares scheme, taking the shallow crustal model at Hekla from Soosalu and Einarsson (1997) as the initial guess. Because we have error bars on the HZ ratio, the data over the frequency band from 0.25–0.35 Hz is weighted more strongly for the data misfit in the inversion.

As shown in Figure 8, the HZ ratios measured at station LARY indicate that the shallow crustal model of Hekla from Sooslau and Einarsson contains shear-wave velocity that is too high by 15% in the upper 1 km of the subsurface. For depths greater than 1 km, the inverted shear-wave velocity is somewhat higher than suggested by the initial model. The lower velocities in the upper 1 km may be the result of station LARY being southwest of the Hekla edifice, within a sediment-filled valley. The ability to gain structural information with HZ ratios derived from ambient noise means that future ANT experiments can use such measurements in addition to the more popular velocity dispersion properties to produce 3D images. An advantage of HZ ratio measurements lies in the ability to obtain uncertainty estimates. For example, the

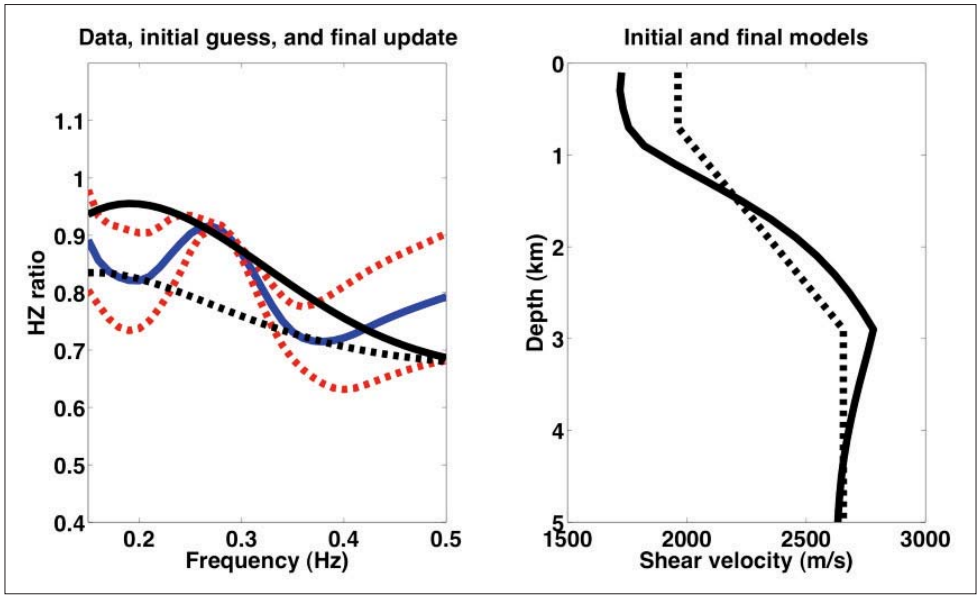

Figure 8. *Quantitative interpretation of the HZ ratio, based on an inversion similar to dispersion curve inversion but for HZ ratio. (left) The mean HZ ratio (solid blue) and one standard deviation error bar (dashed red), the synthetic data from the initial model (dashed black), and the synthetic data from the final model (solid black). (right) The initial model (dashed black) taken from Soosalu and Einarsson (1997) and the final model (solid black).*

inverted HZ ratio in Figure 8 fits the data closely near a frequency of 0.28 Hz because the independent estimates of HZ ratio were highly consistent at that frequency.

Conclusions

We've applied multicomponent PSI to a temporary network of seismometers at Hekla Volcano and inferred structural information from the observed Rayleigh wave ellipticity, or HZ ratio, in cross-correlations. We observed a distinct, narrow frequency band over which the HZ ratio is stable among independent estimates. This demonstrates that the HZ ratio may not always be a pure site effect over all possible frequencies and that a comparison of independent estimates is necessary to establish which frequency bands are the most reliable. The HZ ratio is a new and interesting parameter to analyze in ambient noise cross-correlations. For instance, Baptie (2010) reports on an abrupt change in the relative amplitudes between vertical and radial components of cross-correlations at Montserrat Volcano before and after a dome collapse. Such an abrupt change may indeed be the result of time-varying structure beneath the seismometer, within the volcanic edifice. We can therefore envision monitoring possible temporal changes at Hekla in the future from analyses of the HZ ratio of Rayleigh waves derived from ambient noise. TLE

References

Aki, K. and P. G. Richards, 1980, Quantitative Seismology, W. H. Freeman and Company, New York.

Baptie, B., 2010, Lava dome collapse detected using passive seismic interferometry: Geophysical Research Letters, **37**, L00E10, doi:10.1029/2010GL042489.

Lin, F.-C., M. Moschetti, and M. Ritzwoller, 2008, Surface-wave tomography of the western United States ambient seismic noise: Rayleigh and Love wave phase velocity maps: Geophysical Journal International, **173**, no. 1, 281–298, doi:10.1111/j.1365–246X.2008.03720.x.

Linde, A., K. Agustsson, I. Sacks, and R. Stefansson, 1993, Mechanism of the 1991 eruption of Hekla from continuous borehole strain monitoring: Nature, **365**, no. 6448, 737–740, doi:10.1038/365737a0.

Masterlark, T., M. Haney, H. Dickinson, T. Fournier, and C. Searcy, 2010, Rheologic and structural controls on the deformation of Okmok volcano, Alaska: FEMs, InSAR, and ambient noise tomography: Journal of Geophysical Research, **115**, B2, B02409, doi:10.1029/2009JB006324.

Soosalu, H. and P. Einarsson, 1997, Seismicity around the Hekla and Torfajökull volcanoes, Iceland, during a volcanically quiet period, 1991–1995: Bulletin of Volcanology, **59**, no. 1, 36–48, doi:10.1007/s004450050173.

Tanimoto, T. and S. Tsuboi, 2009, Variational principle for Rayleigh wave ellipticity: Geophysical Journal International, **179**, no. 3, 1658–1668, doi:10.1111/j.1365–246X.2009.04360.x.

Acknowledgments: This work has benefitted from discussions with Wes Thelen, Michael West, Diana Roman, Jim Zollweg, Doug Christensen, Dennis Geist, Cliff Thurber, Kurt Feigl, and Lee Liberty. We thank Guralp Systems for providing help during the field deployment and Halldor Olafsson for assistance in the field.

Corresponding author: matthaney@boisestate.edu